Title: Coastal groundwater model calibration using filtered and amplified hydraulic information retained in the freshwater-saltwater interface

Igor Pavlovskii[1*], Julia A. Cantelon[1], Barret L. Kurylyk[1]

[1]Centre for Water Resources Studies and Department of Civil and Resource Engineering, Dalhousie University, Halifax, Nova Scotia, Canada

* - corresponding author. E-mail:ipavlovs@ucalgary.ca

Abstract

Coastal groundwater flow is driven by an interplay between terrestrial and marine forcing. One of the distinguishing features in these settings is the formation of a freshwater lens due to the density difference between fresh and saline groundwater. The present study uses data collected on Sable Island, Canada – a remote sand island in the northwest Atlantic Ocean – to highlight the potential of exploiting freshwater lens geometry for numerical groundwater flow models calibration in coastal settings. Three numerical, three-dimensional, variable-density groundwater flow models were constructed for different segments of the island, with only one model calibrated using the freshwater-saltwater interface derived from an electromagnetic geophysical survey. The other two (uncalibrated) models with the same parameterisation as the calibrated model successfully reproduced the interpreted interface depth and location of freshwater ponds at different parts of the island. The successful numerical model calibration based solely on the geophysically-derived interface depth is enabled by the interface acting as an amplified version of the water table, which reduces the relative impact of the interpreted depth uncertainty. Furthermore, the freshwater-saltwater interface is far more inertial than the water table, making it less sensitive to short-term forcings. Such "noise-filtering" behaviour enables the use of the freshwater-saltwater interface for calibration even in dynamic settings where selection of representative groundwater heads is challenging. The completed models provide insights into island freshwater lens behaviour and highlight the role of periodic beach inundation and wave overheight in driving short-term water table variability, despite their limited impact on the interface depth.

Keywords

numerical modeling, coastal aquifers, freshwater lens, hydrogeophysics, island hydrogeology

1. Introduction

Coastal zone hydrogeology is emerging as an important research topic within the broader study of changing coastal and marine dynamics (Moore 2010; Oppenheimer et al. 2017; Michael et al. 2017; Santos et al. 2021). This intensified research focus is, in part, due to an increased awareness of the influence of submarine groundwater discharge on coastal water quality (Moore 2006; Sawyer et al. 2016a; Robinson et al. 2018; Threndyle et al. 2022) and projected global population redistribution to coastal zones (Merkens et al. 2016). For example, low-elevation coastal zones already have much higher population densities than the global mean, and this is expected to be exacerbated in future decades (Neumann et al. 2015). The freshwater demand and contamination potential

associated with growing coastal populations provide the impetus to focus research efforts on understanding and properly managing increasingly scarce fresh groundwater resources in coastal zones (Michael et al. 2017). This is arguably most important in small islands as island communities disproportionately rely on groundwater for water supply given the general absence of surface water resources and their limited hydrologic adaptive capacity (Holding and Allen 2015; Werner et al. 2017; Storlazzi et al. 2018; Sharan et al. 2021).

Groundwater flow in coastal zones is driven by the interplay between marine and terrestrial forcing (Santos et al. 2012; Robinson et al. 2018), creating non-obvious cause-and-effect linkages. For example, rising sea levels can cause groundwater levels to rise further inland, threatening infrastructure (Befus et al. 2020; May 2020) and septic water treatment system performance (Cox et al. 2019). Increased terrestrial groundwater recharge can contribute to marine algal blooms by facilitating nutrient export via submarine groundwater discharge (Hu et al. 2006). Short-term storm-surge inundation can adversely affect groundwater quality for years after an event (Cardenas et al. 2015). Also, salinity variations and associated density-dependent flows add extra complexity to groundwater-related processes in coastal zones (Santos et al. 2012; Sawyer et al. 2016b).

Numerical modelling provides an effective tool for understanding groundwater flow processes in coastal zones and for investigating the influence of scenarios such as increased groundwater pumping (Green and MacQuarrie 2014), anthropogenic geologic alterations (Briggs et al. 2021), morphologic change (Holt et al. 2019), water table changes (Befus et al. 2020), sea-level rise (Masterson and Garabedian 2007; Ketabchi et al. 2016), and storm surge inundation (Yang et al. 2013; Holding and Allen 2015; Elsayed and Oumeraci 2018; Paldor and Michael 2021). The primary advantage of numerical modelling is the ability to account for the combined impacts of (real or projected) marine and terrestrial forcings on coupled density-dependent groundwater flow and solute transport processes at specific sites. However, the reliability of numerical model predictions depends on proper model parameterisation.

Calibrating to hydrogeological observations is a common approach for determining hydraulic properties in numerical groundwater flow models (e.g. Anderson et al. 2015). This process involves repeatedly running models with different parameter values until the simulation results and observations converge to an acceptable match. Depending on the scale of the modelling, observations can include a variety of measurable (or otherwise quantifiable) properties or conditions such as hydraulic heads (LaVenue and Pickens 1992), concentrations of different compounds (Schilling et al. 2019), water fluxes, temperatures (Schilling et al. 2019), and ages (Sanford 2011) – or combinations thereof (e.g. Castro and Goblet 2003; Schilling et al. 2019). Despite the potential to calibrate to multiple, complementary datasets, the use of measured hydraulic heads alone remains the most common approach for calibrating groundwater flow models owing to the relative ease of data collection, particularly when well infrastructure is in place (Schilling et al. 2019). However, several factors often undermine the utility of measured hydraulic heads for steady-state model calibration in coastal settings. These include: (1) the relatively high permeability of surficial deposits along high-energy shorelines that decrease lateral hydraulic head gradients, and thus hydraulic head differences, (2) the proximity and strong hydraulic connection to the ocean, which acts as a head boundary condition, further reduces the spatial range in hydraulic heads, (3) transient marine processes (tides, wave action, storm surges) contribute to high temporal variability in hydraulic heads, and (4) hydraulic head

measurements in coastal zones are prone to errors caused by density variations (Carrera et al. 2010). These factors simultaneously complicate the choice of head values for calibration and increase the sensitivity of the calibration results to the chosen head values.

The challenges associated with a steady-state, head-based calibration in coastal settings provide an opportunity for developing an alternative calibration approach. Multiple studies have analysed transient groundwater signals caused by tides, storm surges, and wave action (e.g., Trglavcnik et al. 2018; Xun et al. 2015) to infer subsurface hydraulic properties in coastal settings. However, these methods require additional marine monitoring to measure the transient input signal, and the installation of such instrumentation can be prohibitively challenging and expensive, particularly in high-energy swash zones. Furthermore, high storage coefficients in unconfined aquifers attenuate transient signals (Nielsen 1990), limiting the area of measurable aquifer response. An alternative, but less explored approach relies on the subsurface distribution of fresh and saline groundwater as revealed through geophysical surveys. The exact implementation of such an approach ranges from validating groundwater flow models using geophysical data (Comte and Banton 2007) to coupling hydrogeological and geophysical inversion (Steklova and Haber 2017). While fully-coupled geophysical and hydrogeological inversion remains too computationally intensive to be of practical use in most settings, the addition of geophysically-derived freshwater-saltwater interface depths to observations used during model calibration is a computationally-effective approach to reduce model uncertainty and equifinality (Coulon et al. 2021). However, uncertainty persists regarding whether geophysical data *alone* are sufficient for groundwater flow model calibration, as freshwater-saltwater interface depths derived from geophysical data are inherently imprecise (Carrera et al. 2010).

The overall goal of the present study is to investigate the viability of calibrating a coastal groundwater model using only freshwater-saltwater interface information obtained from geophysics. Given the relative hydraulic inertia of freshwater lenses and saltwater wedges compared to hydraulic heads, this approach may enable calibration to *point-in-time* measurements rather than a long time series of hydraulic head, salinity, or other dynamic conditions that inherently require infrastructure installation and repeated field trips. The specific objectives of this study are to (1) compare the results of a numerical groundwater flow model calibration in a coastal setting using geophysical data alone to results obtained from hydraulic head-based calibration and (2) identify the limitations of geophysics-based calibration. The field data and associated modeling are conducted for a relatively homogeneous sand aquifer that underlies a remote island in the northwest Atlantic Ocean with strong marine forcing.

2. Methods

2.1 Hydraulic theory

Density-dependent flow is one of the factors distinguishing hydrogeological processes in coastal areas from more inland groundwater settings (Jiao and Post 2019). In the case of islands or spits, the density difference between saltwater and freshwater leads to the formation of a “freshwater lens”, in which less dense freshwater forms a distinct lenticular zone that overlies denser saltwater (Figure 1). The relationship between groundwater level and

freshwater lens geometry can be expressed using the classic Ghyben-Herzberg relationship that was initially developed for sand barrier islands along the North Sea coast of Germany (Herzberg 1901):

$$z + h = z\frac{\rho_s}{\rho_f} \text{ or } z = \alpha h \quad (1)$$

where

$$\alpha = \rho_f / [\rho_s - \rho_f] \quad (2)$$

where z is the freshwater-saltwater interface depth below sea level (m), h is the water table elevation above sea level (m), ρ_s is the saltwater density (kg/m^3), ρ_f is the freshwater density (kg/m^3), and α is a dimensionless density ratio. For typical coastal freshwater and saltwater densities (e.g., saltwater of 1027 kg/m^3 at a salinity of 35‰ and temperature within the 20-30°C range) (Sharqawy et al. 2010; Nayar et al. 2016), Equation (1) indicates that the freshwater-saltwater interface depth mirrors the water table elevation, but is amplified by a factor of approximately 37 (i.e., α).

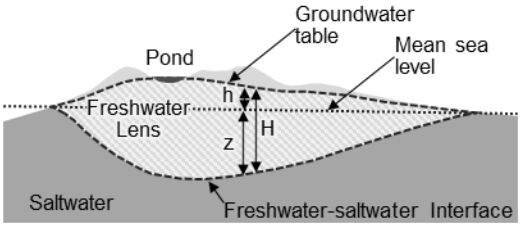

Fig. 1 Conceptual groundwater flow section across an island. Not to scale. Modified from Herzberg (1901). h – water table elevation above sea level; z – freshwater-saltwater interface depth below sea level; H – freshwater lens thickness.

The amplification of the water table reflected in the freshwater-saltwater interface (Figure 1) is the primary factor enabling the use of geophysically-derived interface depths for model calibration instead of or alongside hydraulic head observations. While interface depths interpreted from geophysics may have standard deviations on the order of several metres even in favourable conditions (e.g. Coulon et al. 2021), if an interface follows the Ghyben-Herzberg relationship, the impact of the interface depth error on model calibration has approximately 1/37th the impact of the same error in water table measurements. For example, under this theoretical framework, calibrating a model using an interface estimate that is 3.7 m shallower than its actual position would yield equivalent calibration errors as a water table elevation that is only 10 cm below its actual long-term elevation. Such a small deviation in hydraulic head is within the typical range of short- and long-term head variability and possible measurement errors at many sites.

The amplified relationship noted above has implications for the hydraulic inertia and 'noise filtering' capacity of the interface geometry compared to hydraulic heads, particularly for island aquifers experiencing high-energy marine forcing. Shifting the interface depth to match changing water tables would require displacing 37 times the volume of

water required to cause the change in water table. This suggests that freshwater lenses are not in equilibrium with high-frequency forcing (such signals are filtered) and, thus, the freshwater-saltwater interface is much less dynamic than the water table. In tandem, the amplified and filtered nature of the interface in comparison to hydraulic heads theoretically supports the use of interface-based groundwater model calibration, particularly for settings where the water table is dynamic and close to mean sea level.

2.2 Study site and data sources

The present study uses data from Sable Island (43°55'N, 60º00'W), a narrow sand island in the northwest Atlantic Ocean, approximately 200 km from mainland Canada (Figure 2a). The island represents an emergent portion of the Sable Island bank and is mostly covered by various eolian landforms (Byrne et al. 2014; Eamer et al. 2021). Sable Island consists of a relatively homogeneous sand sequence that transitions into a stiff clay at a depth of ~87 m below the land surface (Jacques McClelland Geosciences inc. 1985). This thick sand sequence has been interpreted as reworked glacial outwash sediments (Byrne et al. 2014). The climate on Sable Island is mild and humid without pronounced seasonality in precipitation (Government of Canada 2020) (Figure 3a). The island hosts several freshwater ponds that provide critical water resources for the unique ecosystem featuring wild horses and endangered seabirds (Freedman 2016; Hennigar and Kennedy 2016). Given the unique ecosystem and long human history (e.g., due to shipwrecks) on Sable Island, it was designated as a Canadian National Park Reserve in 2013 (Freedman 2016).

Previous hydrogeological studies on Sable island (Hennigar 1976; Kennedy et al. 2014; Trglavcnik et al. 2018) confirmed the existence of a distinct freshwater lens and ponds that are hypothesised to be surface manifestations of the water table (Figure 1). Highly dynamic groundwater responses to tides and storms have been confirmed and studied to provide insight into the groundwater system (Trglavcnik et al. 2018). Freshwater lens geometry was recently investigated via multiple geophysical surveys along transects (Figure 2b,2c) perpendicular to the island's long axis (J. Cantelon, Dalhousie University, unpublished thesis data). For each transect, multiple one-dimensional (vertical) transient electromagnetic (TEM) measurements were taken with a WalkTEM (ABEM, Sweden), inverted using the 1D fast AarhusInv inversion code and then stitched together into two-dimensional electrical resistivity cross-sections to distinguish between fresh and saline groundwater. This instrument has been applied to study freshwater lens geometry in other small-island settings (e.g. Briggs et al. 2021). The present study uses a subset of geophysical surveys conducted in July 2020, focusing on two transects separated by approximately 10 km: Main Station (Figure 2a) and Green Plains (Figure 2c). The freshwater-saltwater interface was interpreted for each vertical profile as the depth of the vertical electrical conductivity gradient maximum (Figure 4). Location L1P6B had multiple electrical conductivity gradient peaks (Figure 4a), and thus the shallowest peak was used. Within the flat south beach zone on the Main Station transect, the interface was considered to be located at the surface based on the low electrical resistivity values (Figure 4a). This interface position is consistent with the saline groundwater observed in piezometers in this zone due to periodic inundation by seawater (Kennedy et al. 2014).

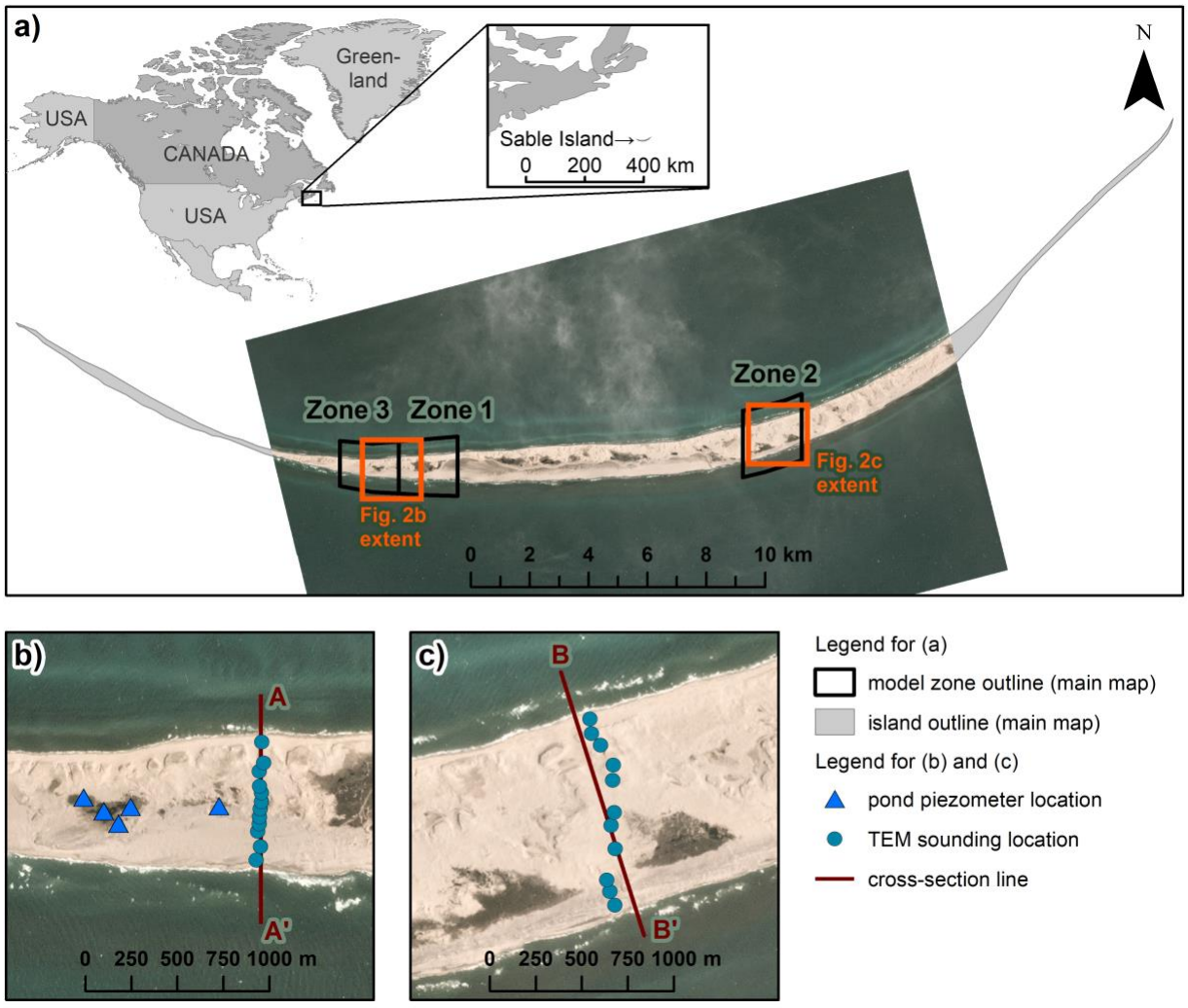

Fig. 2 Study site map: (a) Sable Island overview and its location within Canada (inset) and the location of model zones; (b) location of Main Station geophysical transect and instrumented ponds; (c) location of Green Plains geophysical transect. Background satellite image taken 21 May 2021 (Planet Team, 2018).

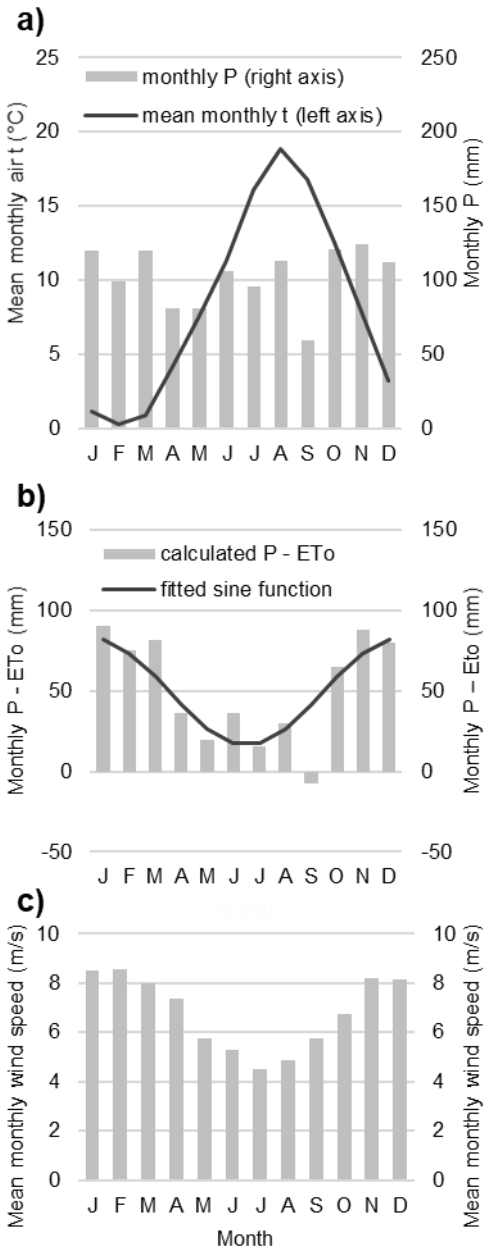

Fig. 3 Study site climate data: (a) mean monthly air temperature and precipitation for the 2015-2019 period on Sable Island (Government of Canada, 2020); (b) mean monthly difference between precipitation and reference evapotranspiration for the 2015-2019 period and fitted sine function; (c) mean monthly wind speed for the 2015-2019 period. P – precipitation; t – air temperature; ETo – reference evapotranspiration.

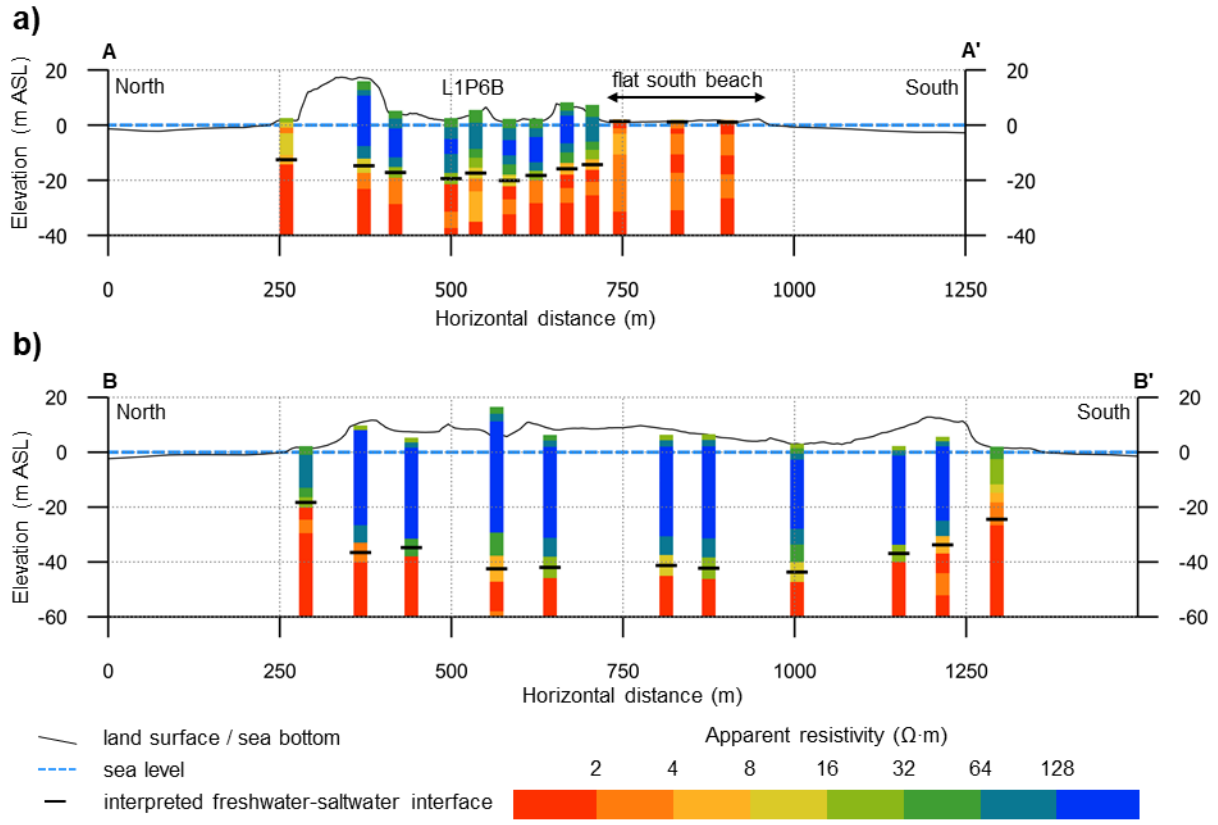

Fig. 4 Geophysical transects obtained from the WalkTEM measurements: (a) Main Station transect and (b) Green Plains transect. The locations of the transects are shown in Figure 2.

In addition to the geophysical data, the present study uses August 2019 – July 2020 groundwater levels from five piezometers installed in pond beds within zone 3 (Figure 2b). Pond bottom elevation at piezometer locations varied in the 0-0.2 m above sea level (ASL) range with an average value below 0.1 m ASL. Piezometers were installed using 1.25" PVC pipe with a 20 cm screened interval covered with a finely meshed sleeve. All piezometers were screened within 0.5 m of the pond bottom and equipped with Solinst Levelogger Junior non-vented water pressure transducers (J. Cantelon, Dalhousie University, unpublished thesis data). Transducer readings were corrected with barometric pressure data recorded at a nearby (~ 1 km) atmospheric pressure transducer installed at a similar elevation.

2.3 Numerical modelling

The overall modeling approach applied in this study is summarised by the following steps/components, which are described in more detail in subsequent sections:

1. Three-dimensional, numerical groundwater flow models were developed for three zones corresponding to different island segments (Figure 2a). All zones used an identical model structure and the same approach for the boundary conditions setup (see Section 2.3.1).

2. Hydraulic conductivity was calibrated for zone 1 using the interpreted interface along the Main Station transect (Figures 2b, 4a). The calibrated hydraulic conductivity values were then applied to zone 2 and zone 3 models to evaluate calibration quality by comparing model results with the interpreted interface depth along the Green Plains transect (zone 2) and the distribution of ponds (zone 3), which were assumed to be surface expressions of the water table. Assessing calibration quality in zones 2 and 3 based on zone 1 calibration relied on the assumption that entire island is underlain by a homogeneous sand aquifer, as proposed in previous field studies (Hennigar 1976).
3. The sensitivity of the water table and freshwater-saltwater interface to the boundary conditions was compared for several scenarios with altered forcing.

2.3.1 Modelling domain and boundary conditions

Three-dimensional numerical groundwater flow and coupled solute transport models were constructed for each zone using FeFlow 7.3 (DHI 2020a). FeFlow is a well-established commercial finite-element modeling package for density-dependent groundwater flow that is frequently applied in coastal aquifer settings (e.g. Smith 2004; Sulzbacher et al. 2012). Models for each zone covered a segment of the island and buffer zones extending 500 m into the sea from both shores (Figure 5a). Each model consists of 40 layers of elements that were 0.5-4 m thick, with the majority of the layers having a fixed thickness of 2 m (Figure 5a). Elements with 0.5 m thickness were located in areas where the top surface elevation cut into the model's grid requiring individual model layers to shift down (Fig. 5a, inset). The triangular prism elements used in the model had variable lateral dimensions: 3-4 m in the 100 m zone along expected lateral boundaries of the freshwater lens; 7-8 m for the rest of the island; 12-20 m for the rest of the sea with the largest element size used in the zone 250 m to 500 m from the island's shore. The purpose of the variable element size was to maintain sufficient resolution in the areas with high salinity gradients, while limiting the overall number of elements and associated computational intensity of the models. Similarly, the separate models for each zone were developed to reduce the computational intensity (processing power and operative memory demands) of each individual model run.

Top surfaces for the models were derived from a 2019 LiDAR survey of the island and nearshore bathymetry for the surrounding waters received from Parks Canada Agency, which oversees the National Park Reserve on the island. Additionally, all nodes above an elevation of 3 m were set to an elevation of 3 m. Such truncation limits the unsaturated zone thickness and contributes to the numerical stability of the model; this should not influence the steady-state model results as measured and modelled hydraulic heads in these zones do not exceed 3 m. The bottom of the model domain was set to a fixed elevation of -84.5 m ASL (above sea level), approximating the transition from sand sediments to the underlying stiff silty clay (Jacques, McClelland Geosciences, 1985).

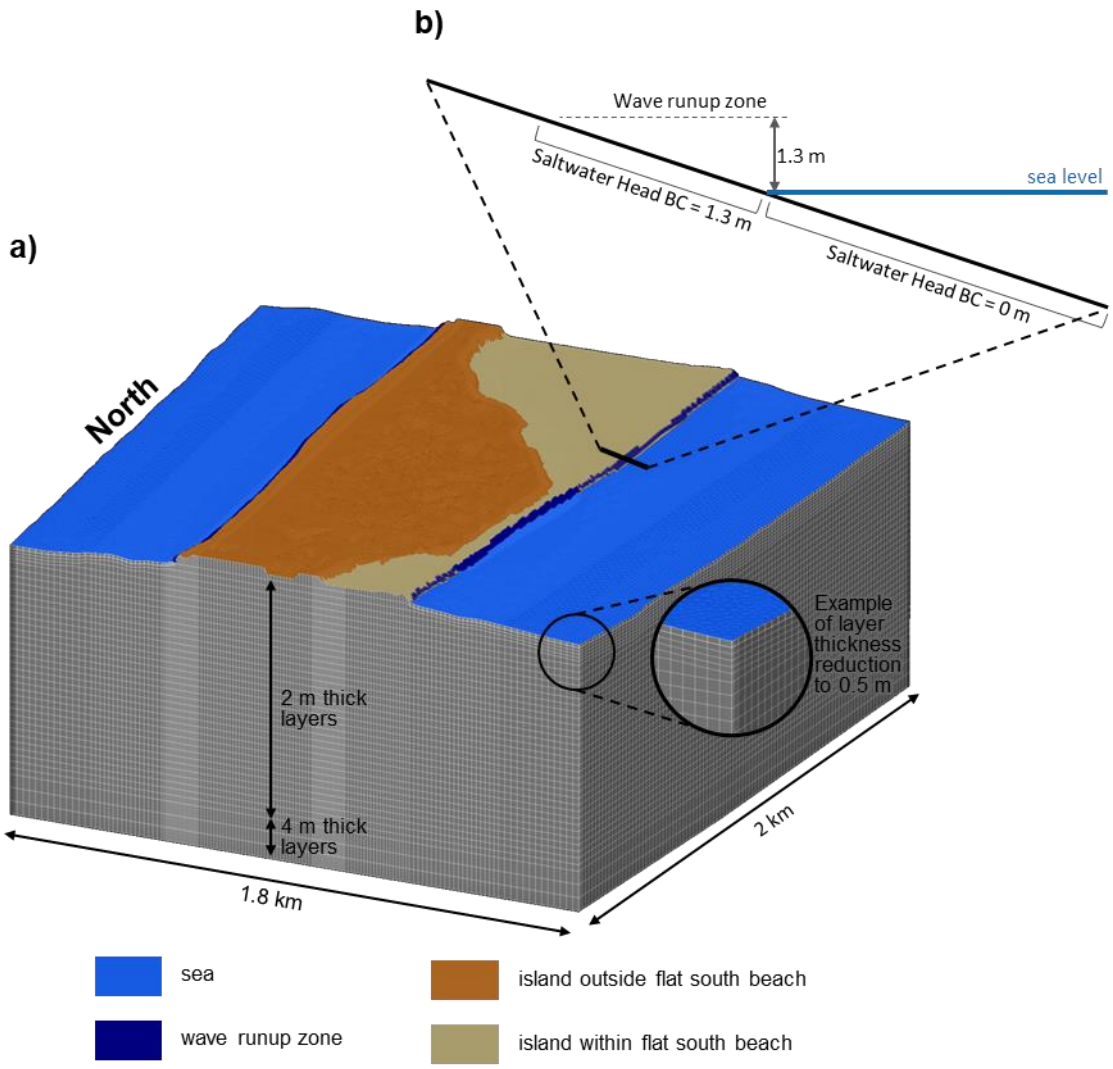

Fig. 5 (a) Model mesh and boundary conditions overview for the zone 1 model; (b) wave overheight boundary condition.

The bottom and sides of each model were assigned no-flow boundaries given the presence of low permeability silty clay at depth and the fact that the model domain was extended significantly offshore to ignore lateral flow at the vertical boundaries. Landward (i.e. cross-shore) sides of the models were oriented north-south – parallel to expected seaward groundwater flow in zone 1 and zone 3, supporting the no-flow boundary assignment (Figure 2a). In the case of zone 2 there is ~20° angle between expected seaward flow and no-flow boundaries. However, the area of interest (geophysical transect) at this zone is located more than 500 m away from these boundaries (Figures 2a, S1b) limiting their effect on the extracted results. The model surface had spatially-varied boundary conditions based on the surface type (Figure 5a). A fixed head boundary of 0 m (sea level) was applied to the submerged, offshore domain surface. Coastal groundwater models often need to account for wave overheight, which refers to a water table increase caused by wave action in the wave run-up zone (Nielsen, 1999) as would be expected in this high-energy wave environment (Smyth and Li 2005). Along the north shore adjacent to the sea, the wave overheight in

the model was specified as a fixed head of 0.75 m; this wave overheight was only applied to locations with surface elevations lower than 0.75 m (Figure 5b). Similarly, along the southern shore adjacent to the sea, a fixed head was set to 1.3 m, where surface elevations were less than 1.3 m (Figure 5b). The two assigned overheight values (0.75 and 1.3 m) were derived in a previous modeling study on the island from observed tidal height and wave run-up (RMC 2018) based on theoretical formulations (Hanslow and Nielsen 1993). The differences in the wave overheight values on the north and south shores arise due to the higher waves consistently observed on the south shore; the resulting cross-shore hydraulic gradient is consistent with observations on barrier islands worldwide (Nielsen 1999).

The fixed head values above are reported as saltwater heads converted to equivalent freshwater heads at boundary condition nodes using the following equation (DHI 2020a):

$$h_{fw} = h_{sw} + \left(\rho_s/\rho_f - 1\right) \cdot (h_{sw} - z) \quad (3)$$

where h_{fw} is the equivalent freshwater head (m), h_{sw} is the saltwater head (m), and z is the nodal elevation (m).

Fixed concentration boundaries with a concentration equivalent to seawater salinity (Table 1) were applied to all nodes with a fixed head boundary (i.e., sea and wave run-up zones, Figure 5a). Additionally, a seawater concentration boundary was applied to the flat south beach zone (Figure 5a) based on the electrical resistivity in geophysical soundings (Figure 4a), repeated flooding incidents revealed in satellite imagery, and groundwater salinity observed in piezometers in this zone (Kennedy et al. 2014). No explicit concentration boundary was applied to the island outside the flat south beach; however, FeFlow assigns a concentration of zero (freshwater) to any water inputs without assigned mass transport boundary conditions.

A specified recharge boundary was applied to all surface elements within the island (both within and outside the flat south beach). Recharge rates were calculated as the difference between recorded precipitation and reference evapotranspiration for the 2015-2019 period (5 years preceding the 2020 geophysical survey). Reference evapotranspiration was calculated from daily meteorological data using an evapotranspiration calculator (FAO 2012) based on the Penman-Monteith equation. Two recharge values were used: a constant recharge of 600 mm (based on mean annual precipitation minus evapotranspiration) and cyclical recharge from a sine function fit to the average monthly differences between precipitation and evapotranspiration (Figure 3b). The specified recharge condition used for each model run is described in the corresponding sections. Other model parameters are indicated in Table 1. Maps showing the spatial distribution of the boundary conditions for all three model zones are provided as Figure S1 of the electronic supplementary material (ESM).

Table 1: Parameters used in the FeFlow model

Parameter name	**Value** (units)
Hydraulic conductivity	calibrated
Seawater salinity	35 ($kg \cdot m^{-3}$)
Porosity	0.3
Specific storage	1×10^{-4} (m^{-1})
Dispersivity (longitudinal)	5 (m)
Dispersivity (transverse)	0.5 (m)

There are separate reasons for using constant, pre-defined values for the porosity, specific storage, and dispersivity. The island is underlain by the unconfined aquifer, which makes the specific storage largely inconsequential. While porosity is an important factor in the transient response in unconfined aquifers, the range of typical porosity values for sand (25-50%, Freeze and Cherry 1979) is dwarfed by the orders of magnitude range of typical hydraulic conductivity values, making the latter the primary factor governing aquifer response. The choice of the dispersivity values is largely governed by the numerical considerations, as is typical in solute transport modelling studies (Smith 2004). Using reduced dispersivity values would require a finer mesh to maintain stability and, consequently, more elements increasing computational intensity. In the case of saltwater wedge formation, the dispersivity primarily affects the thickness of the freshwater-saltwater transition zone (Smith 2004). The transition zone thickness was not the focus of the present study, nor was it directly measured, as the apparent resistivity transition in the geophysical data (Figure 4) is partly an artefact of the smooth inversion.

2.3.2 Model initial conditions, calibration, and evaluation

Although the geometry of the models varied among the three model zones (Figure 2) based on island topography and cross-shore width, the models for all zones used the same set of parameters (Table 1), the same approach to boundary conditions (Figure S1), and were run with the phreatic (unconfined) setting in FeFlow. Combinations of parameters used in different model runs are summarised in Table 2. Initial conditions were established by sequentially running two models: a steady-state model with a horizontal hydraulic conductivity of 5.3×10^{-4} m/s and a vertical hydraulic conductivity of 5.3×10^{-7} m/s followed by a transient model with an isotropic hydraulic conductivity of 5.3×10^{-4} m/s. The hydraulic conductivity estimate (5.3×10^{-4} m/s) for the initial conditions setup was obtained from infiltration tests (Hennigar 1976) and was used in a previous modeling study on the island (Trglavcnik et al. 2018). The reduced vertical hydraulic conductivity was used to maintain numerical stability for the steady-state solution in the initial condition run. While the steady-state run produced a distorted freshwater lens (due to the unrealistically high vertical anisotropy value), the lens presence helped to maintain numerical stability in the beginning of the transient run. The lens' shape was then gradually re-equilibrated to the isotropic hydraulic

conductivity over the course of the transient run. Both initial model runs were completed using a constant recharge rate of 600 mm (precipitation minus reference evapotranspiration, as discussed above). The transient model was run for 10,950 days (≈30 years) to allow the freshwater lens to equilibrate.

Table 2: Overview of parameters used in the different model runs.

Modelling stage	**Model type**	**Model zone**	**Hydraulic conductivity, m/s**	**Recharge**
Initial conditions setup	Steady-state	1, 2, 3	Horizontal: 5.3×10^{-4} Vertical: 5.3×10^{-7}	Constant: 600 mm per year
	Transient		Isotropic: 5.3×10^{-4}	
Calibration	Transient	1	Isotropic: Monte-Carlo values	Cyclical: with a total of 600 mm per year
Model evaluation		2, 3	Isotropic: calibrated value	
Forward runs to evaluate altered forcing effects		1, 2, 3	Isotropic: calibrated value	Cyclical: varied rates (see section 2.3.3)
Model runs to evaluate sensitivity of head-based calibration		zone 3	Isotropic: Monte-Carlo values	Cyclical: with a total of 600 mm per year

After the initial condition setup, the hydraulic conductivity in the zone 1 model was calibrated to replicate the position of the freshwater-saltwater interface along the Main Station transect (Figures 2b, 4a). This was accomplished by setting the target concentration at the interface locations to be 50% of seawater salinity. For the three sounding locations along the flat south beach zone (Figure 4a), the target concentration was set to seawater salinity. Additional observation points at seawater salinity were added 10 m below the interpreted interfaces at these three beach locations to limit the extension of the freshwater lens beneath that flat south beach, as such an extension was not present in the geophysical data (Figure 4a). The weight of these observations along the flat south beach zone was reduced by half (from the original uniform weight at all points) to maintain their overall weight in calibration despite an increase in the number of observations points.

The calibration was completed using a Monte-Carlo approach implemented in FePEST (DHI 2020b), a user interface for the use of PEST (Doherty 2018) in FeFlow. The zone 1 model was run 30 times with randomly generated hydraulic conductivity values from 1×10^{-5} to 1×10^{-2} m/s – a range selected based on the presence of the thick sand sequence beneath the island (Jacques McClelland Geosciences inc. 1985) and typical conductivity values

for sand (Freeze, R.A. and Cherry 1979). Calibration model runs were completed in transient mode with cyclical recharge inputs (Figure 3b). Each model was run for 10,950 days (≈30 years) to allow the freshwater lens to equilibrate. To investigate the impact of simulation time on calibration, an additional set of 30 models was run for 7300 days (≈20 years) for the same set of hydraulic conductivity values. The objective functions in both cases were calculated as the sum of squared errors. The Monte-Carlo approach for calibration was chosen after testing the optimisation approach (i.e., objective function minimum search) in FePEST. It was found that local irregularities in the objective function's shape interfered with optimisation, making its outcome highly sensitive to the initial hydraulic conductivity. The isotropic subsurface was assumed in the Monte-Carlo model runs, similarly to all other modelling stages except the first step of the initial conditions setup (Table 2). An investigation of the impact of anisotropy on model calibration is presented in Appendix 2.

The quality of the zone 1 calibration was evaluated by applying the calibrated hydraulic conductivity to the models for zones 2 and 3. Thus, no calibration was performed at this step for the zone 2 and zone 3 models. These models were run for 10,950 days (≈30 years) with cyclical recharge inputs (Figure 3b). In the zone 2 model, the simulated freshwater-saltwater interface depth (approximated as the concentration isosurface at half of seawater salinity) was compared with the interpreted interface depth from the geophysical survey along the Green Plains transect (Figures 2c, 4b). In the zone 3 model, the simulated water table and pond extents (i.e., where the simulated groundwater level exceeded the land surface elevation) were compared with groundwater levels observed in piezometers screened beneath the pond beds as well as the pond extents visible in satellite images (Figure 2b).

2.3.3 Comparison between the water table and freshwater-saltwater interface dynamics

Three additional model runs for each zone were performed to compare responses of the water table and freshwater-saltwater interface to different forcings:

1) A model run with the recharge rate reduced by a factor of two to evaluate the sensitivity to climate variability;

2) A model run with a 30-day spike in recharge on the "flat south beach" area (Figure 5a), to represent the effects of seawater infiltration from storm surge overtopping that occurs periodically, as revealed in satellite imagery of this beach. This month-long recharge spike was loosely based on field observations of infiltration capacity and ponding depth/duration on this beach; adding this recharge spike increased the total annual recharge along the flat south beach zone to 1500 mm (i.e., an extra 900 mm recharge was added over the 30-day interval);

3) A model run with the wave overheight boundary conditions removed to consider the freshwater lens conditions without the effects of waves increasing the groundwater heads along the shore. This involved removing corresponding fixed head and fixed concentration boundaries and resulted in freshwater recharge in the former wave runup zone It is not expected that waves would disappear completely, and thus, the purpose of this scenario is to evaluate the general sensitivity of the freshwater lens to changes in wave height – a highly variable forcing.

These additional model runs used simulated hydraulic heads and salinities at the end of runs with the calibrated hydraulic conductivity as initial conditions. Each model was run for 10,950 days (≈30 years) to allow the freshwater

lens to equilibrate with the changed boundary conditions, but only the data spanning the last two years of the simulations was used for the analysis.

Additionally, the model's sensitivity to head-based calibration was evaluated by applying the calibration procedure described above (Section 2.3.2) for the zone 3 model, but with hydraulic heads at the piezometers (Fig. 2b) as the calibration target rather than the interpreted interface from geophysics. In this case, the Monte-Carlo analysis was repeated twice using two different sets of groundwater levels from piezometers beneath the ponds (Figure 2b) as the calibration target and the root mean squared error as the objective function. The first run used mean water levels for August 2019 – July 2020 (i.e., averaged over 1 year), while the second used the mean water levels for August 2019 (a period with relatively low and stable levels). The objective function in these Monte-Carlo simulations was calculated as the sum of squared errors with the same weight was applied to all head measurements.

3. Results

3.1 Groundwater flow model calibration and evaluation results

The objective function used for the freshwater-saltwater interface-based calibration has a minimum, indicating a successful calibration was achieved for a hydraulic conductivity of ~ 3.1×10^{-4} m/s (27 m/day) (Figure 6), herein referred to as the calibrated hydraulic conductivity. The 20- and 30-year runs had nearly identical objective function values at this hydraulic conductivity value, indicating that the model had effectively reached steady state by the end of 20-year runs. However, the divergence of the objective function values between the 20- and 30-year runs at lower hydraulic conductivities (e.g., 1×10^{-5} m/s) suggests that the freshwater lens geometry is not fully equilibrated in these lower conductivity cases (Figure 6).

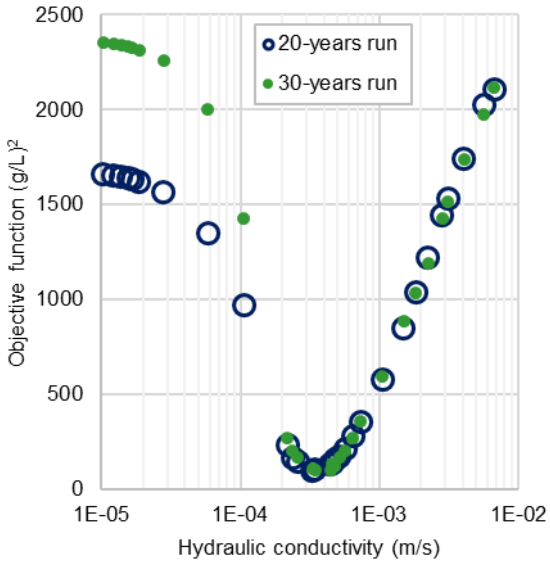

Fig. 6 Results of the Monte-Carlo calibration based on the freshwater-saltwater interface depth along the Main Station transect (zone 1, Figures 2). These results reveal the relationship between the objective function (sum of squared errors) and hydraulic conductivity.

For the runs with calibrated hydraulic conductivity, the simulated freshwater-saltwater interface depth distribution generally matched the interface depths interpreted from geophysical data along both the Main Station (zone 1 model) and Green Plains (zone 2 model) transects (Figure 7), although only the former was used for calibration and the concentration isosurface at half of seawater salinity were used as the calibration target rather than the interpreted interface depth itself. The distribution of the modelled concentrations along the geophysical transects (Figure 4) is provided as Figure S2 of the ESM. Satellite images for Sable Island are often obscured by heavy fog and clouds; however, the zone 3 model successfully reproduced the location of the ponds visible in the clear satellite image for May 21st, 2021 (Planet Team 2017) (Figure 8a). The simulated groundwater levels at all piezometer locations are close to the observed mean annual values of 0.61-0.76 m; however, the simulated seasonal water level variation is much smaller than the observed seasonal variation. Additionally, simulated groundwater levels notably lack the distinct short-term spikes evident in the observed hydraulic head data (Figure 8b). The high temporal variability in observed water levels not captured by the model indicates that the modelled pond extents represent annual averages as opposed to conditions on a specific date.

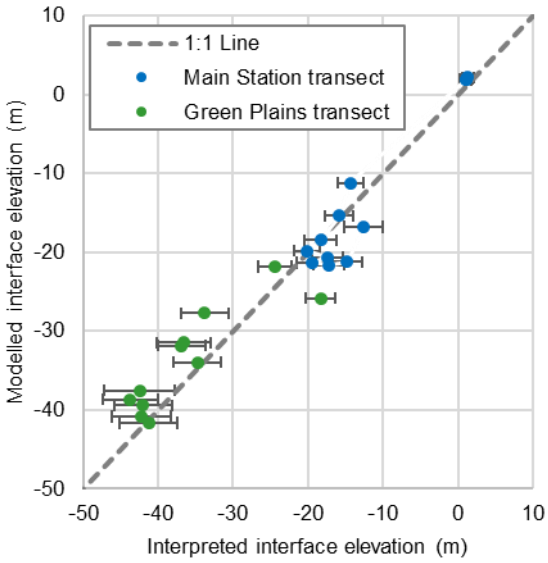

Fig. 7 Modelled vs. interpreted freshwater-saltwater interface elevations along the TEM transects. Error bars shows size of the elements produced by the geophysics inversion (Fig. 4). Locations of transects are shown on Fig. 2

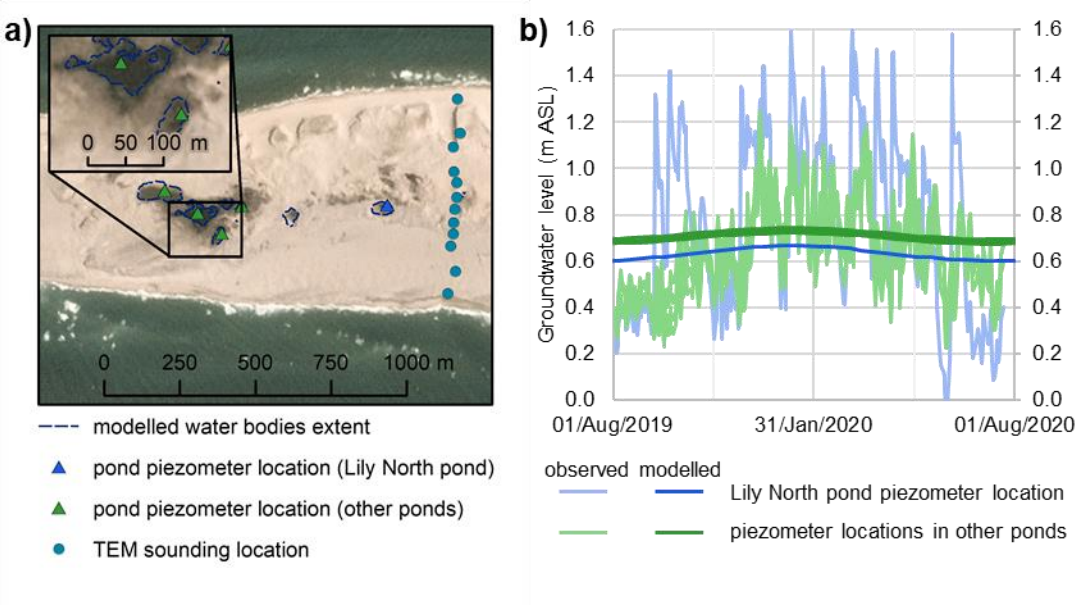

Fig. 8 (a) Modelled water body extents within the zone 3 model at the end of the simulation. Modelled water bodies extents are based on the areas where modelled groundwater level exceeds the surface elevation; (b) observed and modelled groundwater elevation in the pond piezometers.

3.2 Comparison between the water table and freshwater-saltwater interface dynamics

The water table and interface dynamics in response to altered boundary conditions, including storm surge inundation (Section 2.3.3), were compared to assess the relative dynamics of these two hydraulic energy indicators in the zone 3 model. Both the water table and the freshwater-saltwater interface responded to the recharge reduction by a factor of two (Figure 9). The modelled water tables (Figure 9a) displayed seasonal periodicity due to the imposed recharge cycle (Figure 2b) and were lowered by approximately 16 cm on average (22-25% reduction relative to the original head). Freshwater lens geometry showed high inertia as re-equilibration to reduced recharge took over a decade. Due to the amplified response of the freshwater-saltwater interface, the overall lens thickness at pond locations decreased from 13-17 m (for original recharge rate) to 8-10 m for the lower recharge (Figure 9b). The modelled decreases in lens thicknesses are broadly consistent with the analytical solution for freshwater lens geometry underlying strip islands (Fetter 1972), which indicates that the water table elevation and lens thickness are both a function of the square root of recharge. Thus, reducing the recharge rate by 50% would theoretically lead to a water table elevation and freshwater lens depth (below sea-level) reduction by a factor of 1.4 (i.e., $\sqrt{2}$).

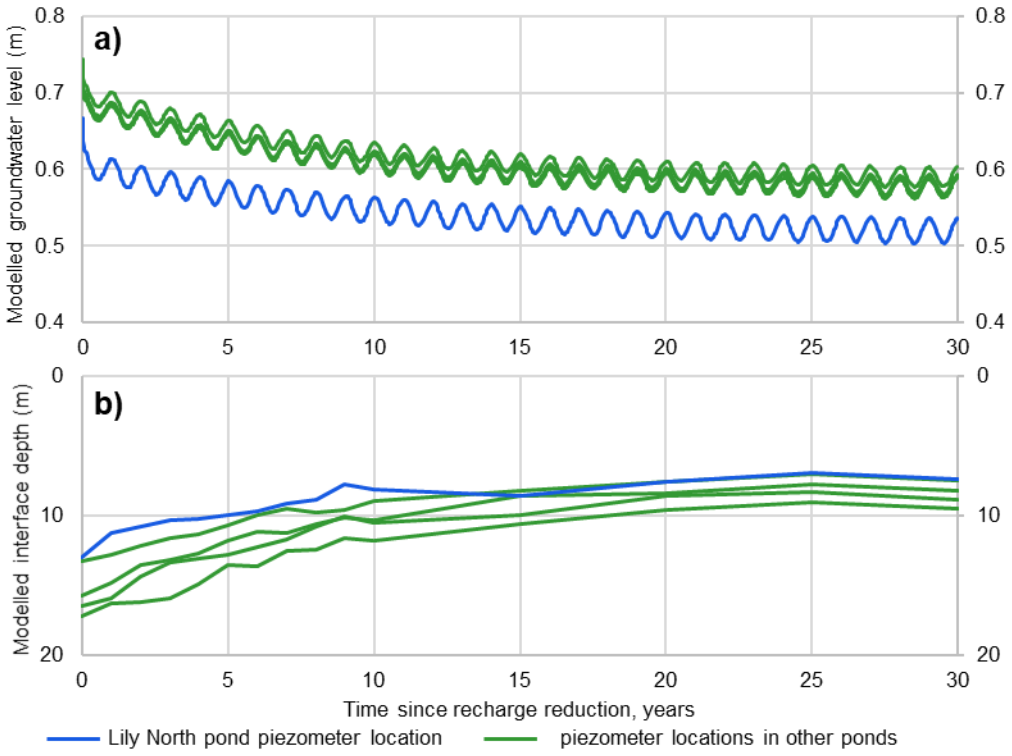

Fig. 9 Modelled response to a recharge reduction by a factor of two at pond piezometer locations: (a) groundwater table and (b) freshwater-saltwater interface beneath these piezometers.

The modelled water table and freshwater-saltwater interface exhibited divergent responses to the short-term spike in saltwater recharge representing the effects of coastal flooding on the flat south beach zone. The water table by the pond piezometers (i.e., outside the flat south beaches zone where flooding was imposed) immediately responded to the increase in recharge from seawater flooding with a pronounced spike that quickly dissipated when recharge returned to background values (Figure 10b). In contrast to the water table, the freshwater-saltwater interface at the same locations remained relatively stable throughout and after the period with increased recharge (Figure 10e).

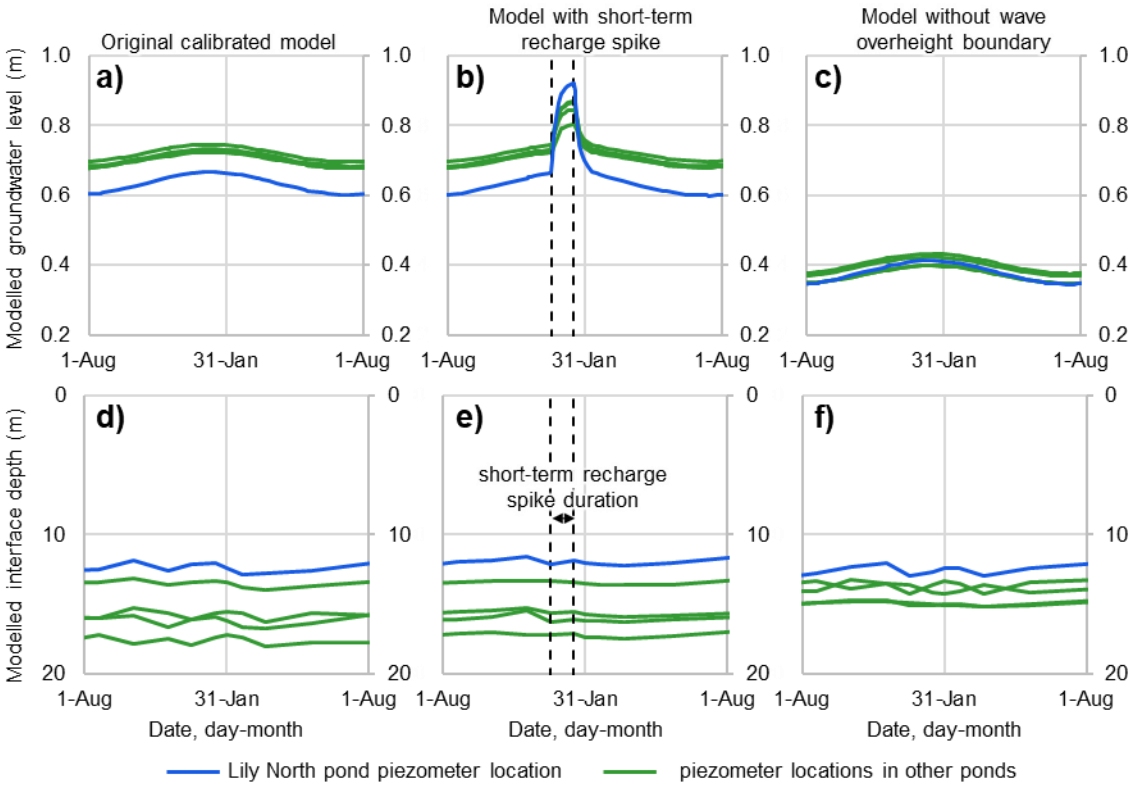

Fig. 10 Sensitivity of the modeled groundwater table (a-c) and freshwater-saltwater interface (d-f) at pond piezometer locations in the zone 3 model (model output spanning the last two years of the 30-year simulation): (a) (d) default calibrated model; (b) and (e) scenario with a short-term spike in recharge within the flat south beach zone; (c) and (f) scenario with switched off wave overheight boundary conditions.

Removing the wave overheight boundary conditions resulted in a modelled groundwater level decline of approximately 20 cm at pond piezometer locations (Figure 10c) relative to the simulations with the wave overheight boundary conditions imposed (Figure 10a). However, the average depth of the freshwater-saltwater interface at pond piezometer locations (Figure 10f) remained broadly the same as with the wave overheight boundary condition (Figure 10d). Removing the wave overheight boundary conditions did reduce the range of the freshwater-saltwater interface depths at the pond piezometer locations due to the removal of the head gradient between the wave overheight boundary conditions on the different sides of the island (i.e., the freshwater lens became more symmetrical).

Model calibration based on groundwater levels alone was highly sensitive to the choice of the observation period. The hydraulic conductivity value corresponding to the lowest values of the objective function (root mean squared error of the groundwater level) varied by an order of magnitude depending on whether it was based on the observed mean groundwater level between August 2019 – July 2020 or the mean groundwater level of August 2019 (Figure 11). For the model run based on July 2019-August 2020 water levels, the minimum of the objective function corresponded to a hydraulic conductivity value of 3.5×10^{-4} m/s, which is similar to the value (3.1×10^{-4} m/s) obtained

from calibration to the freshwater-saltwater interface (Figure 8). In contrast, the use of the August 2019 hydraulic head as the calibration target results in an objective function minimum for a hydraulic conductivity value that is one order of magnitude larger (3×10^{-3} m/s).

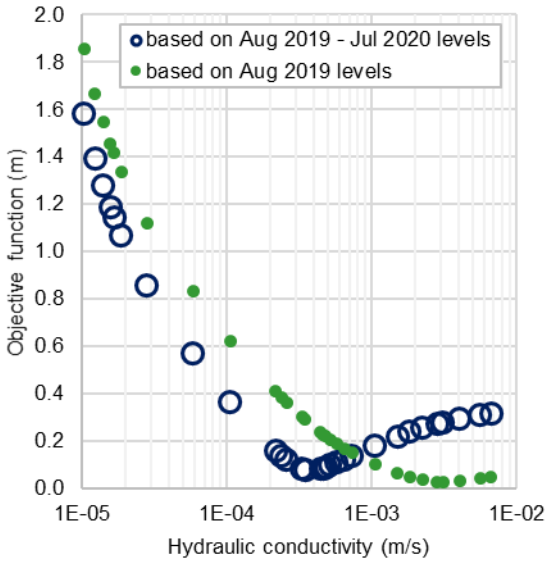

Fig. 11 Results of the Monte-Carlo simulations (objective function vs. hydraulic conductivity) based on the groundwater levels at pond piezometer locations for levels averaged over 1 year (*blue*) and over 1 month with relatively low and stable levels (*green*). The objective function was the root mean squared error.

4. Discussion

While previous coastal modelling studies have applied a combination of hydraulic head and geophysical data to calibrate or assess numerical models (e.g., Comte et al. 2010; Sulzbacher et al. 2012), advantages and limitations of calibrating to geophysical data alone has not been as well studied. To address this knowledge gap, this study considered the performance of model calibrations based on either hydraulic head data in piezometers or freshwater-saltwater interface depths interpreted from geophysics. The primary differences between these two calibration targets are their relative sensitivities to transient forcing and relative signal magnitudes as discussed below.

Modelling results highlight that the perception of the saltwater-freshwater interface as an inverted and amplified water table is not representative for all scenarios through time, even in the case of a uniform subsurface. Rather, the exact relationship between the water table elevation and freshwater-saltwater interface depth is strongly dependent on the forcing involved. In the case of permanent recharge reductions, the re-equilibration of the water table and freshwater-saltwater interface to new conditions occurred in parallel (Figure 9), supporting the paradigm of the interface as an amplified and reflected water table. In contrast, the effects of the simulated spike in beach recharge (attributed to short-term beach inundation) immediately manifested themselves in the water table (Figure 10b), but did not strongly influence the freshwater-saltwater interface (Figure 10e). Similarly, the removal of the wave overheight boundary conditions reduced the water table elevation around the pond piezometers, but did not cause a

proportional reduction in the freshwater-saltwater interface depth (Figure 10f). Two possible factors contribute to the freshwater-saltwater interface depth's limited sensitivity to wave overheight. First, changing the base level for the freshwater lens equilibration would cause an identical vertical shift in both the water table and the freshwater-saltwater interface. However, even a 1 m shift, which would be well within the margin of error for the interpreted interface depth (Figure 7), would cause a large relative change in groundwater elevations relative to the absolute datum. A second possible factor is the spatial variation and contributions of different boundary conditions. Even with the wave overheight boundary condition active, the freshwater lens geometry is still affected by the sea boundary condition (Figure 5). As a result, the difference in responses may indicate different relative contributions of proximal (wave overheight) and distal (sea) boundary conditions to the water table elevation and the freshwater-saltwater interface depth.

The contrasting response of the water table and freshwater-saltwater interface to different forcing further highlights the utility of the latter for groundwater model calibration. The sensitivity of groundwater levels to transient forcing (beach inundation, wave action) can noticeably bias calibration. For example, groundwater levels modelled in the case with no wave overheight (Figure 10c) are similar to levels observed in August 2019 (Figure 8b). Using these levels during calibration yields hydraulic conductivity values an order of magnitude higher than those obtained using the mean annual water levels (Figure 11) or the freshwater-saltwater interface (Figure 6). In contrast, the limited sensitivity of the freshwater-saltwater interface to both short-term beach inundation and removal of wave overheight (Figures 10e, 10f) makes the interface geometry a preferred option for pseudo-steady-state calibration based on point-in-time data.

Despite the advantages listed above, hydraulic conductivity calibration based on the freshwater-saltwater interface is likely to have limited applicability in coastal settings with lower hydraulic conductivity than this study site. The divergence between the objective function values for different model run times (Figure 6) suggests that the freshwater lens takes more than 20 years to equilibrate at hydraulic conductivities below 1×10^{-4} m/s. Even for the calibrated hydraulic conductivity of 3.1×10^{-4} m/s, the freshwater-saltwater interface depth approached its final position only 15 years after the recharge was reduced by a factor of two (Figure 9). These still represent relatively high hydraulic conductivities compared to many coastal settings (e.g. Zamrsky et al. 2020), and in lower conductivity settings, model equilibration may take much longer. As a result, calibration in such settings would require an assumption about the stability of boundary conditions (recharge rate, recharge distribution, and relative sea-level) over many decades, if not centuries. Furthermore, geophysics-derived resistivity distributions are often more complex to interpret in heterogeneous coastal environments (King et al. 2021), which would make it more challenging to identify interface depths when compared to the relatively homogeneous sand aquifer setting investigated in this study. Consequently, the choice of targets for numerical groundwater flow model calibration (freshwater-saltwater interface, hydraulic heads, or both) requires taking into account site-specific conditions. Steady-state calibration to both observed freshwater-saltwater interface position and hydraulic heads can be counterproductive if these are not mutually consistent: e.g., if observed heads are defined by a short-term forcing

that does not affect the more inertial interface depth (Figures, 10b, 10e) or if the freshwater-saltwater interface is still equilibrating with the current forcings due to low hydraulic conductivity (Figure 6).

The developed model provided insights into the behaviour of the freshwater lens beneath Sable Island and potentially beneath similar sand barrier islands and spits elsewhere (e.g., Stutz and Pilkey 2001). The observed short-term spikes in the pond water level (Figure 8b) are consistent with the response to the inundation of adjacent flat beaches (Figure 10b). That is, coastal flooding and a concomitant increase in seawater recharge along the edge of the freshwater lens is sufficient to temporarily elevate the inland fresh water table, an effect previously reported at different frequencies or spatial considerations in the context of long-term sea level rise (Gulley et al. 2016) and for interface migration during storm surge overtopping (Paldor and Michael 2021). The plausibility of this scenario is further supported by similarities between modelled water table response and observed water table dynamics. For example, the magnitudes of water level spikes in the piezometer at Lily North are higher in both the observations (Figure 8b) and model simulations (Figure 10b) than the water level spikes in other pond piezometers located farther from the south beach and the associated marine forcing (Figure 8a).

Another finding concerns the importance of the wave overheight in maintaining the freshwater lens' water table elevation (Figures 10a, 10c). In addition to model results, the hypothesis about the role of waves in maintaining groundwater levels is supported by the observation that the period of lower observed groundwater levels in June-August (Figure 8b) occurs in the months with lowest mean wind speeds (Figure 3c), which are directly linked to wave height. While this evidence remains circumstantial as the seasonal variation in wind speed also correlates with the seasonal variation in recharge (Figure 3b), the role of waves in maintaining freshwater levels may be an important, but hitherto often overlooked factor in coastal settings. It is important to note that considering seasonal recharge changes *alone* in the modelling (Figure 2b) was not enough to reproduce the full magnitude of seasonal change in the water table elevations (Figure 8b), suggesting seasonality in marine processes is also important. At the same time, the importance of wave overheight is likely limited to sites with small hydraulic head differentials, for example, relatively small islands formed by sediments with high hydraulic conductivity. These processes (i.e., the influence of infiltration during coastal flooding and seasonal and short-term variations in wave overheight) will be further investigated in subsequent studies through the integration of more detailed and sustained field observations (groundwater and pond levels and wave dynamics) and numerical modelling in zone 3 (Figure 2).

Lastly, the successful application of the hydraulic conductivity value calibrated only for zone 1 to zone 2 (Figure 7) and zone 3 (Figure 8a) models highlights the predictive power of the numerical modelling and confirms the consistency in the hydraulic conductivity across the island. The zone 2 model also successfully captured the much deeper interface position at this portion of the island, demonstrating the model's ability to extrapolate beyond the calibrated range.

5. Conclusions

The present study demonstrated that the calibration of a groundwater flow model using geophysically-derived freshwater-saltwater interface depths alone is both a possible and useful option for a relatively homogenous narrow

sand island with a distinct freshwater lens. The model's hydraulic conductivity that was calibrated to reproduce the freshwater-saltwater interface depths along a geophysical transect was successfully used to replicate interface depths along another transect over 10 km away. Furthermore, the same calibrated hydraulic conductivity value applied to another three-dimensional zone successfully reproduced the distribution of surface water features, interpreted as locations where simulated head exceeds the land surface elevation. Finally, the modelled water table closely approximated the mean annual observed groundwater levels not used in calibration. These lines of evidence support the efficacy of groundwater model calibration solely based on the geophysical interface depths.

Further analysis indicated that, despite the high uncertainty in interface depth, the interface-based calibration offers distinct advantages over groundwater level-based model calibration at the study site. The relationship between the upper (water table) and lower (interface) boundaries of a Ghyben-Herzberg freshwater lens leads to a model calibration that is far less sensitive to errors in interface depth than errors in hydraulic head measurements. Also, unlike water levels, the freshwater-saltwater interface at the study site has greater hydraulic inertia and thus limited sensitivity to short-term variations in wave overheight or spikes in recharge following coastal flooding. As a result, for the purpose of calibration, the freshwater-saltwater interface can be considered an amplified and noise-filtered version of the water table, leading to a higher signal-to-noise ratio in the data being calibrated to. These advantages appear to be limited to settings with high hydraulic conductivity, where freshwater lens equilibration occurs at time scales that support steady-state assumptions for the boundary conditions during calibration.

This study's modelling and data analysis further indicate that beach inundation and associated saltwater recharge drive short-term spikes in fresh groundwater levels at the study site. Also, the present study identified wave overheight (and, by extension, the marine and meteorological processes driving it) as an important factor in maintaining fresh groundwater levels. These same processes are likely to apply in similar coastal settings (e.g., narrow sandy barrier islands and spits) and warrant further consideration in field programs and numerical modelling efforts.

6. Acknowledgements

Dr. Dan Kehler (Parks Canada Agency) and Mr. Terry Hennigar are particularly thanked for their invaluable technical support and local knowledge and experience relating to Sable Island. We also thank two anonymous reviewers for their comments that helped to improve the readability of the manuscript.

Funding Information and Conflicts of Interest

This research was undertaken thanks in large part to funding from the Canada First Research Excellence Fund through the Ocean Frontier Institute (postdoctoral fellowship to I. Pavlovskii) and financial contributions and logistical support from Parks Canada Agency. Field campaigns were supported by a MEOPAR early-career award/grant to B. Kurylyk and scholarship/grant support to J. Cantelon from NSERC, Killam, the Geological Society of America, and the Canadian Water Resources Association Dillon Scholarship. B. Kurylyk is supported through the Canada Research Chairs Program.

Authors declare no conflicts of interest.

Appendix 1

A separate set of zone 1 Monte-Carlo model runs was performed to evaluate the impact of anisotropy on calibration. The zone 1 model was run 100 times with randomly generated horizontal and vertical hydraulic conductivity values from 1×10^{-4} to 1×10^{-3} m/s. The vertical and horizontal hydraulic conductivity values were generated independently of each other resulting in an anisotropic model. The narrow hydraulic conductivity range was selected based on the results of the isotropic Monte-Carlo runs showing the objective function minimum at a hydraulic conductivity value of ~ 3.1×10^{-4} m/s (Figure 6). These runs used the same boundary conditions, objective function, and initial conditions as zone 1 Monte-Carlo runs described in Section 2.3.2.

The objective function minimum in the anisotropic runs was achieved for the 2.5×10^{-4} to 4×10^{-4} m/s range of horizontal hydraulic conductivity values, which is in the vicinity of the 3.1×10^{-4} m/s value obtained through isotropic calibration (Figure 12). The corresponding range of vertical hydraulic conductivity values is wider but still reasonably well constrained between 3×10^{-4} and 9×10^{-4} m/s. Similarly low objective functions values can be obtained for different combinations of vertical and horizontal conductivity values. These combinations follow an inverse relationship: lower values of horizontal hydraulic conductivity require higher values of vertical hydraulic conductivity to maintain the same objective function value.

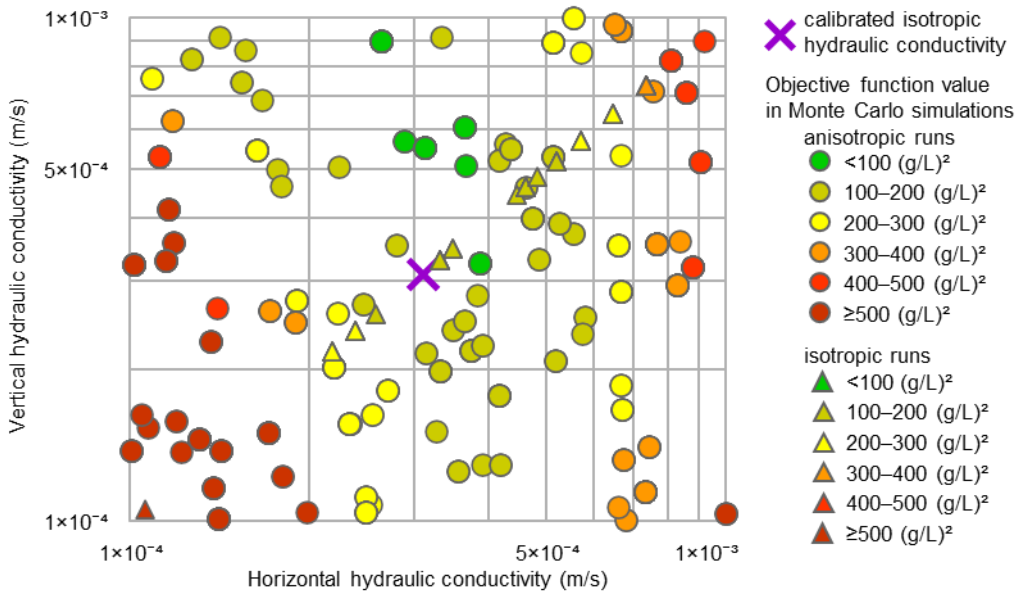

Fig. 12 Results of the Monte-Carlo calibration (*colours* indicate objective function values) based on the freshwater-saltwater interface depth along the Main Station transect (zone 1) with enabled anisotropy in hydraulic conductivity. The objective function is a sum of squared errors. Results for the isotropic runs are from Figure 6.

The Monte-Carlo runs highlight the non-uniqueness of the anisotropic calibration which likely arises from the non-negligible vertical flow component for a freshwater lens in a thick permeable aquifer. Such vertical flows can invalidate commonly used analytical solutions (e.g., Fetter 1972) for freshwater lens geometry. At the same time, the

flow remains predominantly horizontal as indicated by the steep gradient between optimal vertical and horizontal conductivity values (Figure 12). That is, any change in horizontal hydraulic conductivity requires a larger change in the vertical hydraulic conductivity in the opposite direction to maintain a similar lens thickness.

A trend towards lower objective function values for cases where vertical hydraulic conductivity is larger than horizontal (Figure 12) minimises the effect of non-uniqueness on the calibration results used in the main body of the present paper. Such a combination of parameters is unlikely given the sediment lithology and depositional setting at the study site, making the isotropic case a reasonable approximation.

Supplementary figures

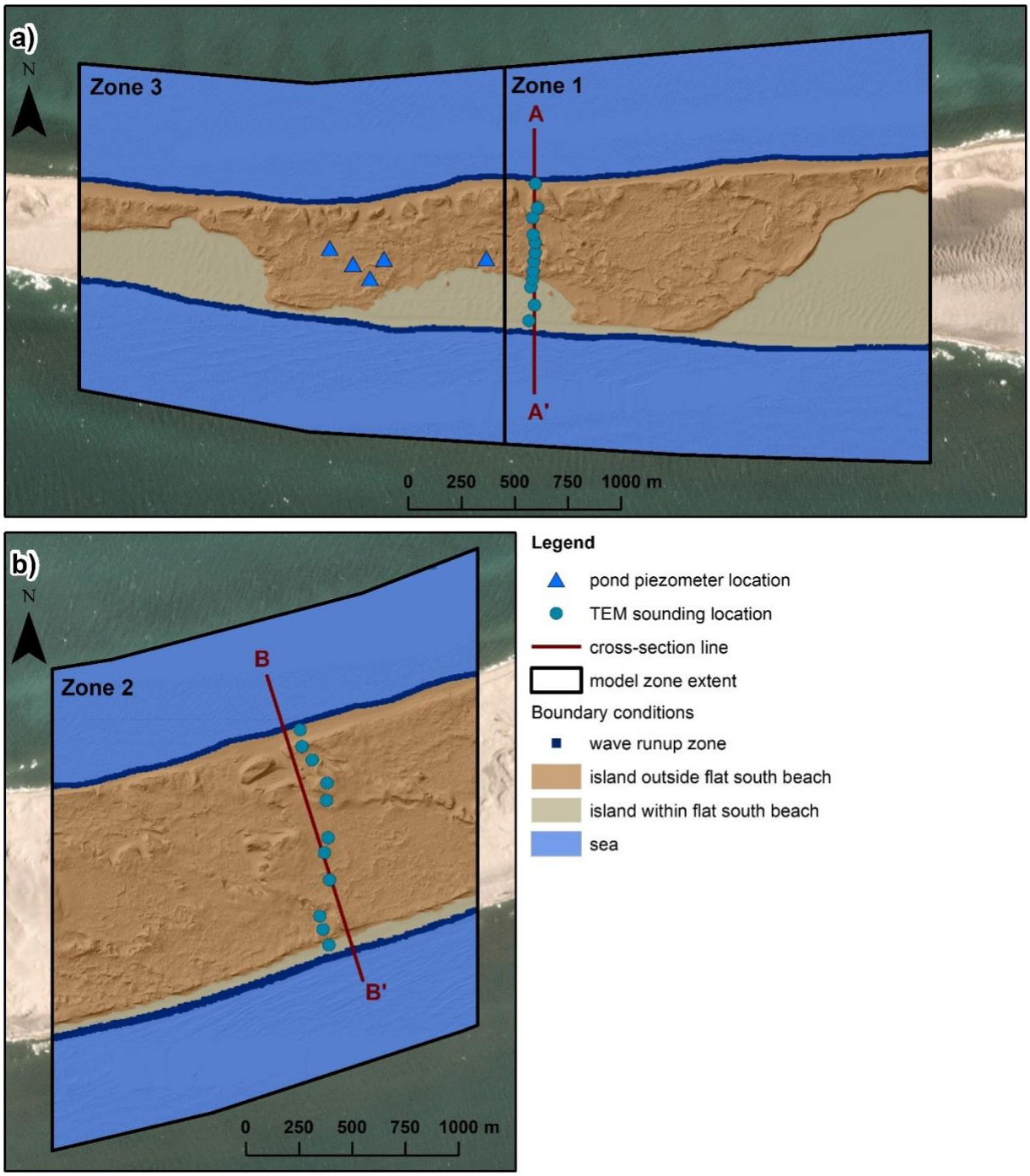

Fig. S1 Boundary conditions maps for (a) zone 1 and zone 3 models; (b) zone 2 model. Background satellite image taken 21 May 2021 (Planet Team, 2018).

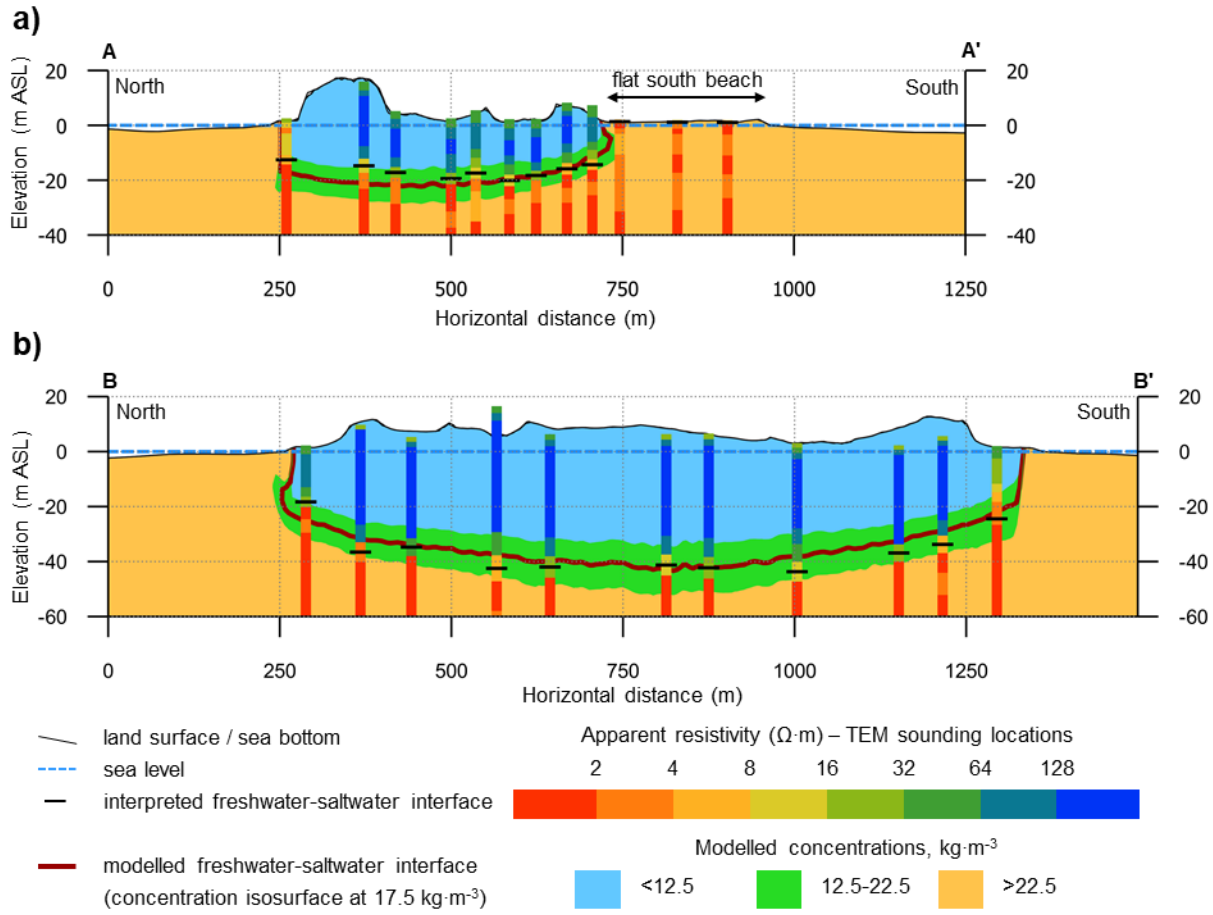

Fig. S2 Modelled freshwater-saltwater interface along geophysical transects: (a) Main Station transect and (b) Green Plains transect. The locations of the transects are shown in Figure 2.

References

Anderson MP, Woessner WW, Hunt RJ (2015) Applied Groundwater Modeling, 2nd Editio. Elsevier

Befus KM, Barnard PL, Hoover DJ, et al (2020) Increasing threat of coastal groundwater hazards from sea-level rise in California. Nat Clim Chang 10:946–952. https://doi.org/10.1038/s41558-020-0874-1

Briggs MA, Cantelon JA, Kurylyk BL, et al (2021) Small atoll fresh groundwater lenses respond to a combination of natural climatic cycles and human modified geology. Sci Total Environ 756:143838. https://doi.org/10.1016/j.scitotenv.2020.143838

Byrne M-L, Freedman B, Colville D (2014) The Geology of Sable Island and Evolution of the Sable Island Bank. In: An Ecological and Biodiversity Assessment of Sable Island. pp 17–33

Cardenas MB, Bennett PC, Zamora PB, et al (2015) Devastation of aquifers from tsunami-like storm surge by Supertyphoon Haiyan. Geophys. Res. Lett. 42:2844–2851

Carrera J, Hidalgo JJ, Slooten LJ, Vázquez-Suñé E (2010) Computational and conceptual issues in the calibration of seawater intrusion models. Hydrogeol J 18:131–145. https://doi.org/10.1007/s10040-009-0524-1

Castro MC, Goblet P (2003) Calibration of regional groundwater flow models: Working toward a better understanding of site-specific systems. Water Resour Res 39:1–25. https://doi.org/10.1029/2002WR001653

Comte J-C, Banton O (2007) Cross-validation of geo-electrical and hydrogeological models to evaluate seawater intrusion in coastal aquifers. Geophys Res Lett 34:L10402. https://doi.org/10.1029/2007GL029981

Comte JC, Banton O, Join JL, Cabioch G (2010) Evaluation of effective groundwater recharge of freshwater lens in small islands by the combined modeling of geoelectrical data and water heads. Water Resour Res 46:. https://doi.org/10.1029/2009WR008058

Coulon C, Pryet A, Lemieux JM, et al (2021) A framework for parameter estimation using sharp-interface seawater intrusion models. J Hydrol 600:. https://doi.org/10.1016/j.jhydrol.2021.126509

Cox AH, Loomis GW, Amador JA (2019) Preliminary Evidence That Rising Groundwater Tables Threaten Coastal Septic Systems. J Sustain Water Built Environ 5:04019007. https://doi.org/10.1061/jswbay.0000887

DHI (2020a) FEFLOW, version 7.3 (Update 5), Finite-Element Simulation System for Subsurface Flow and Transport Processes. DHI Institute for Water and Environment

DHI (2020b) FePest – FEFLOW Parameter Estimation, Version 7.3

Doherty J (2018) PEST, Model-Independent Parameter Estimation User Manual. Watermark Numerical Computing, Brisbane, Australia

Eamer JBR, Didier D, Kehler D, et al (2021) Multi-decadal coastal evolution of a North Atlantic shelf-edge vegetated sand island – Sable Island, Canada. Can J Earth Sci 1–37. https://doi.org/10.1139/cjes-2020-0194

Elsayed SM, Oumeraci H (2018) Modelling and mitigation of storm-induced saltwater intrusion: Improvement of the resilience of coastal aquifers against marine floods by subsurface drainage. Environ Model Softw 100:252–277. https://doi.org/10.1016/j.envsoft.2017.11.030

FAO (2012) FAO Food Outlook: Global Market Analysis. Rome

Fetter CW (1972) Position of the saline water interface beneath oceanic islands. Water Resour Res 8:1307–1315. https://doi.org/10.1029/WR008i005p01307

Freedman B (ed) (2016) Sable Island: Explorations in Ecology and Biodiversity

Freeze, R.A. and Cherry JA (1979) Groundwater. Prentice-Hall Inc., Englewood Cliffs

Government of Canada (2020) Historical Climate Data (Sable Island Station). http://climate.weather.gc.ca/. Accessed 23 Dec 2020

Green NR, MacQuarrie KTB (2014) An evaluation of the relative importance of the effects of climate change and groundwater extraction on seawater intrusion in coastal aquifers in Atlantic Canada. Hydrogeol J 22:609–623. https://doi.org/10.1007/s10040-013-1092-y

Gulley JD, Mayer AS, Martin JB, Bedekar V (2016) Sea level rise and inundation of island interiors: Assessing impacts of lake formation and evaporation on water resources in arid climates. Geophys Res Lett 43:9712–9719. https://doi.org/10.1002/2016GL070667

Hanslow D, Nielsen P (1993) Shoreline Set-Up on Natural Beaches. J Coast Res 1–10

Hennigar TW (1976) Water Resources and Environmental Geology of Sable Island, Nova Scotia. Report No. 76-1

Hennigar TW, Kennedy GW (2016) The precarious freshwater resources of Sable Island, Nova Scotia, Canada: Occurrence and management considerations. Proc Nov Scotian Inst Sci 48:331. https://doi.org/10.15273/pnsis.v48i2.6662

Herzberg A (1901) Die Wasserversorgung einiger Nordseebäder. J für Gasbeleuchtung und Wasserversorgung 815–819

Holding S, Allen DM (2015) Wave overwash impact on small islands: Generalised observations of freshwater lens response and recovery for multiple hydrogeological settings. J Hydrol 529:1324–1335. https://doi.org/10.1016/j.jhydrol.2015.08.052

Holt T, Greskowiak J, Seibert SL, Massmann G (2019) Modeling the Evolution of a Freshwater Lens under Highly Dynamic Conditions on a Currently Developing Barrier Island. Geofluids 2019:. https://doi.org/10.1155/2019/9484657

Hu C, Muller-Karger FE, Swarzenski PW (2006) Hurricanes, submarine groundwater discharge, and Florida's red tides. Geophys Res Lett 33:1–5. https://doi.org/10.1029/2005GL025449

Jacques McClelland Geosciences inc. (1985) Project G042 Report to Centre for Marine Geology, Dalhousie University and Atlantic Geoscience Centre on 1985 Sable Island Borehole Project

Jiao J, Post V (2019) Coastal Hydrogeology. Cambridge University Press

Kennedy GW, Drage J, Hennigar TW (2014) Groundwater Resources of Sable Island , Nova Scotia Open File Report ME 2014-001 Halifax , Nova Scotia. Halifax

Ketabchi H, Mahmoodzadeh D, Ataie-Ashtiani B, Simmons CT (2016) Sea-level rise impacts on seawater intrusion in coastal aquifers: Review and integration. J Hydrol 535:235–255. https://doi.org/10.1016/j.jhydrol.2016.01.083

King J, Mulder T, Essink GO, Bierkens MFP (2021) Joint estimation of groundwater salinity and hydrogeological parameters using variable-density groundwater flow, salt transport modelling and airborne electromagnetic surveys. Adv Water Resour 160:104118. https://doi.org/10.1016/j.advwatres.2021.104118

LaVenue AM, Pickens JF (1992) Application of a coupled adjoint sensitivity and kriging approach to calibrate a groundwater flow model. Water Resour Res 28:1543–1569. https://doi.org/10.1029/92WR00208

Masterson JP, Garabedian SP (2007) Effects of sea-level rise on ground water flow in a coastal aquifer system. Ground Water 45:209–217. https://doi.org/10.1111/j.1745-6584.2006.00279.x

May C (2020) Rising groundwater and sea-level rise. Nat Clim Chang 10:889–890. https://doi.org/10.1038/s41558-020-0886-x

Merkens JL, Reimann L, Hinkel J, Vafeidis AT (2016) Gridded population projections for the coastal zone under the Shared Socioeconomic Pathways. Glob Planet Change 145:57–66. https://doi.org/10.1016/j.gloplacha.2016.08.009

Michael HA, Post VEA, Wilson AM, Werner AD (2017) Science, society, and the coastal groundwater squeeze. Water Resour Res 53:2610–2617. https://doi.org/10.1002/2017WR020851

Moore WS (2010) The effect of submarine groundwater discharge on the ocean. Ann Rev Mar Sci 2:59–88. https://doi.org/10.1146/annurev-marine-120308-081019

Moore WS (2006) The role of submarine groundwater discharge in coastal biogeochemistry. J Geochemical Explor 88:389–393. https://doi.org/10.1016/j.gexplo.2005.08.082

Nayar KG, Sharqawy MH, Banchik LD, Lienhard JH (2016) Thermophysical properties of seawater: A review and new correlations that include pressure dependence. Desalination 390:1–24. https://doi.org/10.1016/j.desal.2016.02.024

Neumann B, Vafeidis AT, Zimmermann J, Nicholls RJ (2015) Future coastal population growth and exposure to sea-level rise and coastal flooding - A global assessment. PLoS One 10:. https://doi.org/10.1371/journal.pone.0118571

Nielsen P (1990) Tidal dynamics of the water table in beaches. Water Resour Res 26:2127–2134. https://doi.org/10.1029/WR026i009p02127

Nielsen P (1999) Groundwater dynamics and salinity in coastal barriers. J Coast Res 15:732–740

Oppenheimer M, Glavovic BC, Hinkel J, et al (2017) Sea Level Rise and Implications for Low-Lying Islands, Coasts and Communities. In: Pörtner HO, Roberts DC, Masson-Delmotte V, et al. (eds) IPCC Special Report on the Ocean and Cryosphere in a Changing Climate. IPCC, pp 321–446

Paldor A, Michael HA (2021) Storm Surges Cause Simultaneous Salinization and Freshening of Coastal Aquifers,

Exacerbated by Climate Change. Water Resour Res 57:1–14. https://doi.org/10.1029/2020WR029213

Planet Team (2017) Planet Application Program Interface: In Space for Life on Earth

RMC (2018) Sable Island Hydrological Model. Phase I and II Program Development. Kingston, Canada

Robinson CE, Xin P, Santos IR, et al (2018) Groundwater dynamics in subterranean estuaries of coastal unconfined aquifers: Controls on submarine groundwater discharge and chemical inputs to the ocean. Adv Water Resour 115:315–331. https://doi.org/10.1016/j.advwatres.2017.10.041

Sanford W (2011) Calibration of models using groundwater age. Hydrogeol J 19:13–16. https://doi.org/10.1007/s10040-010-0637-6

Santos IR, Chen X, Lecher AL, et al (2021) Submarine groundwater discharge impacts on coastal nutrient biogeochemistry. Nat Rev Earth Environ 2:307–323. https://doi.org/10.1038/s43017-021-00152-0

Santos IR, Eyre BD, Huettel M (2012) The driving forces of porewater and groundwater flow in permeable coastal sediments: A review. Estuar Coast Shelf Sci 98:1–15. https://doi.org/10.1016/j.ecss.2011.10.024

Sawyer AH, David CH, Famiglietti JS (2016a) Continental patterns of submarine groundwater discharge reveal coastal vulnerabilities. Science (80-) 353:705–707. https://doi.org/10.1126/science.aag1058

Sawyer AH, Michael HA, Schroth AW (2016b) From soil to sea: the role of groundwater in coastal critical zone processes. Wiley Interdiscip Rev Water 3:706–726. https://doi.org/10.1002/wat2.1157

Schilling OS, Cook PG, Brunner P (2019) Beyond Classical Observations in Hydrogeology: The Advantages of Including Exchange Flux, Temperature, Tracer Concentration, Residence Time, and Soil Moisture Observations in Groundwater Model Calibration. Rev Geophys 57:146–182. https://doi.org/10.1029/2018RG000619

Sharan A, Lal A, Datta B (2021) A review of groundwater sustainability crisis in the Pacific Island countries: Challenges and solutions. J Hydrol 603:127165. https://doi.org/10.1016/j.jhydrol.2021.127165

Sharqawy MH, Lienhard V JH, Zubair SM (2010) Thermophysical properties of seawater: A review of existing correlations and data. Desalin Water Treat 16:354–380. https://doi.org/10.5004/dwt.2010.1079

Smith AJ (2004) Mixed convection and density-dependent seawater circulation in coastal aquifers. Water Resour Res 40:1–16. https://doi.org/10.1029/2003WR002977

Smyth CE, Li MZ (2005) Wave-current bedform scales, orientation, and migration on Sable Island Bank. J Geophys Res C Ocean 110:1–12. https://doi.org/10.1029/2004JC002569

Steklova K, Haber E (2017) Joint hydrogeophysical inversion: state estimation for seawater intrusion models in 3D. Comput Geosci 21:75–94. https://doi.org/10.1007/s10596-016-9595-y

Storlazzi CD, Gingerich SB, Van Dongeren A, et al (2018) Most atolls will be uninhabitable by the mid-21st century because of sea-level rise exacerbating wave-driven flooding. Sci Adv 4:1–10. https://doi.org/10.1126/sciadv.aap9741

Stutz ML, Pilkey OH (2001) A Review of Global Barrier Island Distribution. J Coast Res 15–22

Sulzbacher H, Wiederhold H, Siemon B, et al (2012) Numerical modelling of climate change impacts on freshwater lenses on the North Sea Island of Borkum using hydrological and geophysical methods. Hydrol Earth Syst Sci 16:3621–3643. https://doi.org/10.5194/hess-16-3621-2012

Threndyle RE, Kurylyk B, Huang Y, et al (2022) CrAssphage as an indicator of groundwater-borne pollution in coastal ecosystems. Environ Res Commun 2:0–31. https://doi.org/10.1088/2515-7620/ac693a

Trglavcnik V, Morrow D, Weber KP, et al (2018) Analysis of Tide and Offshore Storm-Induced Water Table Fluctuations for Structural Characterization of a Coastal Island Aquifer. Water Resour Res 54:2749–2767. https://doi.org/10.1002/2017WR020975

Werner AD, Sharp HK, Galvis SC, et al (2017) Hydrogeology and management of freshwater lenses on atoll islands: Review of current knowledge and research needs. J Hydrol 551:819–844. https://doi.org/10.1016/j.jhydrol.2017.02.047

Xun Z, Chao S, Ting L, et al (2015) Estimation of aquifer parameters using tide-induced groundwater level measurements in a coastal confined aquifer. Environ Earth Sci 73:2197–2204. https://doi.org/10.1007/s12665-014-3570-5

Yang J, Graf T, Herold M, Ptak T (2013) Modelling the effects of tides and storm surges on coastal aquifers using a coupled surface-subsurface approach. J Contam Hydrol 149:61–75. https://doi.org/10.1016/j.jconhyd.2013.03.002

Zamrsky D, Karssenberg ME, Cohen KM, et al (2020) Geological Heterogeneity of Coastal Unconsolidated Groundwater Systems Worldwide and Its Influence on Offshore Fresh Groundwater Occurrence. Front Earth Sci 7:1–23. https://doi.org/10.3389/feart.2019.00339